

*Selected papers presented at the 15th Symposium of Magnetic Measurements and Modelling SMMM'2025*

## Validation of the Jiles–Atherton Model of the Magnetic Hysteresis Loop of Grain-Oriented Electrical Steel

R. SZEWCZYK<sup>a,\*</sup> AND J. PYTLÍK<sup>b</sup>

<sup>a</sup>*Institute of Metrology and Biomedical Engineering, Faculty of Mechatronics, Warsaw University of Technology, św. A. Boboli 8, 02-525 Warsaw, Poland*

<sup>b</sup>*Department of Physics, VSB — Technical University of Ostrava, 17. listopadu 2172/15, 708 00 Ostrava-Poruba, Czech Republic*

Doi: [10.12693/APhysPolA.149.S126](https://doi.org/10.12693/APhysPolA.149.S126)

\*e-mail: [roman.szewczyk@pw.edu.pl](mailto:roman.szewczyk@pw.edu.pl)

The paper evaluates different variants of the Jiles–Atherton model of magnetic hysteresis, focusing on the experimental verification of the model's hysteretic component characteristics. Five modelling strategies were examined: the original Jiles–Atherton model, a modified variant proposed by Venkataraman et al., the approach of Cheng and coauthors, as well as the modification proposed by Pytlík et al. Grain-oriented electrical steel was selected as a benchmark due to the complex shape of both its anhysteretic magnetization and hysteresis loop. Quantitative evaluation of the obtained results enables the assessment of the quality of hysteresis behaviour reproduction in anisotropic electric steel. Moreover, it enables verification of the functional properties of different modelling approaches used for inductive components in electric devices.

topics: magnetic hysteresis, Jiles–Atherton model, grain-oriented electrical steel

### 1. Introduction

Magnetic hysteresis can be observed as changes in the shape of the  $B(H)$  loop of ferromagnetic materials, where  $B$  is the flux density and  $H$  is the magnetizing field, in both the increasing and decreasing phases. This phenomenon is especially important in the case of high-permeability soft magnetic materials, where the nonlinearity and hysteresis of the  $B(H)$  characteristic determine the behaviour of inductive components [1].

Magnetic hysteresis has been investigated since its discovery by Sir James Alfred Ewing in 1881 [2]. However, it should be highlighted that a generalized model of magnetic hysteresis, quantitatively describing the macroscopic magnetic behaviour of a wide range of isotropic and anisotropic materials, excitation conditions, and coupled physical effects, has not yet been presented [3]. Moreover, recent analyses indicate that a comprehensive understanding of the physical mechanisms underlying magnetic, magnetostrictive, and magnetoelastic effects would necessitate descriptions that extend into quantum physics of solid state [4].

Nevertheless, due to its ability to connect macroscopic magnetization to simplified representations of key domain processes, the Jiles–Atherton model [5] has become one of the most commonly utilized tools for magnetic hysteresis modelling in

technical applications [6, 7]. In particular, this model is widely applied in the design and optimization of inductive components such as transformers [8], chokes [9], actuators [10], and sensors [11], where a reliable reproduction of the hysteresis loop is required for loss estimation and performance prediction. The importance of quantitative hysteresis modelling is especially visible in the case of grain-oriented electrical steels [12] used as core materials in power transformers and other energy conversion devices. In such cases, the anisotropic characteristic of grain-oriented electric steel leads to sophisticated shapes of the magnetic hysteresis loop [13], especially when the material is magnetized perpendicularly to the rolling direction.

Understanding the Jiles–Atherton model requires taking into account both its anhysteretic and hysteretic parts [5]. The quantitative description of the anhysteretic magnetization curve has been previously validated for both isotropic and anisotropic materials [14, 15]. However, different approaches to modelling the hysteresis loop have been proposed, including the original formulation of the Jiles–Atherton model and several later variants that modify the irreversible magnetization equation or correct earlier editorial and numerical inconsistencies. At the same time, various numerical strategies have been applied to solve the model equations and identify the model parameters, mostly based on optimization using stochastic and bio-inspired

methods [16]. However, a systematic verification of the different Jiles–Atherton variants against demanding experimental data for grain-oriented electrical steels, carried out with controlled numerical accuracy and a unified parameter identification methodology, has not yet been presented.

This paper is intended to fill this gap. The proposed approach utilizes previously validated descriptions of anhysteretic magnetization [15] and focuses on the experimental verification of several hysteretic formulations of the Jiles–Atherton model for grain-oriented electrical steel. A two-step identification procedure [17] is employed, in which the anhysteretic parameters are first determined, and the hysteretic parameters are subsequently optimized using experimental  $B(H)$  loops measured for the material magnetized in the transverse direction. The efficiency of the analyzed modelling approaches is evaluated using quantitative modelling quality indicators. The obtained results provide guidelines for balancing computational cost and accuracy when optimizing inductive component cores in power engineering.

## 2. Experimental measurements

The modelling was based on experimental results of measuring the magnetic hysteresis loop  $B(H)$ , previously presented in the literature [18]. The investigated material was a high-permeability, grain-oriented Fe–Si electrical steel with approximately 3% silicon by mass. The sheet had dimensions  $0.3 \times 30 \times 300 \text{ mm}^3$  and a standard surface coating typical of transformer core materials.

The magnetic hysteresis loop was obtained using a single sheet tester based on a Magneto-Optical Kerr Effect (MOKE) microscope and magnetometer [18, 19]. The sheet was placed inside a magnetic frame with a laminated yoke closing the flux path, and driving and pickup coils were wound around it. The sheet sample was cut with its long axis perpendicular to the rolling direction of the original electrical steel. Before measurement, the sheet was demagnetized. A triangular magnetic field waveform at a frequency of 0.5 Hz and an amplitude of 200 A/m was then applied along the sample length, thereby magnetizing the material in the transverse direction.

## 3. General concept of the Jiles–Atherton model

In Jiles–Atherton model, the effective magnetic field magnetizing the material,  $H_e$ , is described as [5]

$$H_e = H + \alpha M, \quad (1)$$

where  $H$  is the external magnetic field,  $M$  is the total magnetization of the material, and  $\alpha$  is the Bloch’s domain coupling factor. Next, the anhysteretic magnetization  $M_{ah}$  is calculated from the following equation [15, 20]

$$M_{ah}(H) = M_s \frac{\int_0^\pi d\theta e^{\frac{1}{2}(E(1)+E(2))} \sin(\theta) \cos(\theta)}{\int_0^\pi d\theta e^{\frac{1}{2}(E(1)+E(2))} \sin(\theta)}, \quad (2)$$

where  $M_s$  is the saturation magnetization of the material. For the axial anisotropy in the material, the energy components are given as [15]

$$E_{\text{axial}}(1) = \frac{H_e}{a} \cos(\theta) - \frac{K_{an}}{\mu_0 M_s a} \sin^2(\psi - \theta), \quad (3)$$

$$E_{\text{axial}}(2) = \frac{H_e}{a} \cos(\theta) - \frac{K_{an}}{\mu_0 M_s a} \sin^2(\psi + \theta), \quad (4)$$

whereas for grain-oriented anisotropy, the energy components are [21]

$$E_{\text{axial}}(1) = \frac{H_e}{a} \cos(\theta) - \frac{K_{an}}{\mu_0 M_s a} \times \left[ \cos^2(\psi - \theta) \sin^2(\psi - \theta) + \frac{\sin^4(\psi - \theta)}{4} \right], \quad (5)$$

$$E_{\text{axial}}(2) = \frac{H_e}{a} \cos(\theta) - \frac{K_{an}}{\mu_0 M_s a} \times \left[ \cos^2(\psi + \theta) \sin^2(\psi + \theta) + \frac{\sin^4(\psi + \theta)}{4} \right]. \quad (6)$$

In (3)–(6),  $K_{an}$  is the dominant value of the average energy density of the axial magnetic anisotropy,  $a$  quantifies the density of the domain walls,  $\mu_0$  is the magnetic constant, and  $\psi$  is the angle between the direction of magnetizing field  $H$  and the material’s magnetization easy axis.

It should be highlighted that when the dominant value of the average axial magnetic anisotropy energy density  $K_{an}$  is equal to 0, (2) reduces to the Langevin equation in both component cases [5, 22], i.e.,

$$M_{ah}(H) = M_s \left[ \coth\left(\frac{H_e}{a}\right) - \frac{a}{H_e} \right], \quad (7)$$

representing the anhysteretic magnetization curve of an isotropic magnetic material. Next, hysteresis is introduced to the model by the differential equation, generally stated as

$$\frac{dM}{dH} = f\left(M_{ah}, \frac{dM_{ah}}{dH}, k, c\right), \quad (8)$$

where  $k$  describes the average energy required to break the pinning sites and  $c$  quantifies the reversibility of the magnetization process. Moreover, phenomenologically justified parameters are commonly applied, namely  $\delta$  (determining if the magnetizing field  $H$  increases or decreases) and parameter  $\delta_M$  (guaranteeing that the incremental susceptibility remains positive) [23]. Finally, after solving the differential equation (8), the magnetic

flux density  $B$  in the material is calculated on the basis of the following equation

$$B_{ah}(H) = \mu_0 (M_{ah}(H) + H). \quad (9)$$

It should be highlighted that in the anisotropic case there is no antiderivative for integrations in (2). However, from a numerical point of view, solving (2)–(6) is relatively simple. It can be done effectively by the trapezoid method or the adaptive Simpson method. On the other hand, solving (8) may be challenging and requires the use of the Runge–Kutta method with advanced sampling and approximations [24].

Identifying the parameters of the Jiles–Atherton model is commonly carried out in the optimization process during the minimization of the target function  $T$ . Here,

$$T = \sum_{i=1}^n \left[ B_{\text{meas}}(H_i) - B_{\text{sym}}(H_i) \right]^2, \quad (10)$$

where  $B_{\text{meas}}$  are the results of experimental measurements, and  $B_{\text{sym}}$  are the results from modelling for a given set of parameters; both quantities were evaluated at the same magnetizing field  $H_i$ . Due to the sophisticated form of the target function  $T$  and the possibility of local minima, the differential evolution algorithm is considered an efficient optimization method. In the presented research, the default differential evolution optimisation method [25] was used, where the generation of new candidate solutions involved adding a scaled difference of two random population members to a third one, and then mixing this result with the current solution, retaining it only if it performed better. The number of population members, NP, was equal to 420.

#### 4. Investigated variants of the Jiles–Atherton model-based descriptions of magnetic hysteresis

During the tests, five variants of the Jiles–Atherton model were tested:

- (i) the original Jiles–Atherton model [5];
- (ii) the Jiles–Atherton model updated by Cheng et al. [26], where  $\frac{dM_{ah}}{dH}$  is used instead  $\frac{dM_{ah}}{dH_e}$ ;
- (iii) the Jiles–Atherton model updated by Venkataraman et al. [27] (bulk ferromagnetic model), where anhysteretic magnetization is modified to include domain wall motion effects and a more physically consistent treatment of irreversible magnetization;
- (iv) the DIMFH version of the Jiles–Atherton model [28] (DIMFH — differential isotropic model of ferromagnetic hysteresis), in which the derivative  $\frac{dM}{dH}$  is redefined through a thermodynamically consistent differential framework that ensures smooth transitions

between reversible and irreversible magnetization and eliminates the non-physical discontinuities present in the original Jiles–Atherton formulation;

- (v) the Jiles–Atherton model updated by Xue et al. [29], where the effective field  $H_e$  is redefined to include stress-dependent effects and a modified coupling parameter to better represent magneto–mechanical behaviour in soft magnetic materials.

The key differential equations describing the five variants of the Jiles–Atherton model are presented in Table I. To understand the most important changes these variants introduced, the parts of equations concerning the irreversible magnetization  $M_{irr}$  were isolated by zeroing out the parameter  $c$  (magnetization reversibility).

In Table I, the following mathematical convention was used

$$M_\alpha = \frac{dM_{ah}}{dH}, \quad (11)$$

$$\delta = \begin{cases} +1, & H_{end} \geq H_{start} \\ -1, & H_{end} < H_{start} \end{cases} \quad (12)$$

$$(M_{ah} - M)_\delta = \begin{cases} \max(M_{ah} - M, 0), & \delta = +1, \\ \min(M_{ah} - M, 0), & \delta = -1. \end{cases} \quad (13)$$

It should be highlighted that modifications of the Jiles–Atherton model also significantly influence its numerical complexity. The simplest and most numerically stable implementation is the one used in DIMFH. On the other hand, the model variant proposed by Xue et al. [29] is the most numerically sophisticated.

The coefficient of determination,  $R^2$ , was used to quantitatively assess the modelling quality. This metric compares the modelled flux density  $B$  with the experimental measurements over the analyzed quarter of the hysteresis loop  $B(H)$ . The  $R^2$  coefficient is calculated as

$$R^2 = 1 - \frac{SS_{res}}{SS_{tot}}. \quad (14)$$

The residual sum of squares  $SS_{res}$  quantifies the unexplained variance between the model and experimental data,

$$SS_{res} = \sum_{i=1}^n \left[ B_{\text{meas}}(H_i) - B_{\text{sym}}(H_i) \right]^2, \quad (15)$$

and the total sum of squares,  $SS_{tot}$ , represents the total variance present in the experimental data

$$SS_{tot} = \sum_{i=1}^n \left[ B_{\text{meas}}(H_i) - \bar{B}_{\text{meas}} \right]^2. \quad (16)$$

In these equations,  $B_{\text{meas}}$  denotes the measured flux density,  $B_{\text{sym}}$  is the flux density predicted by the model, and  $\bar{B}_{\text{meas}}$  is the arithmetic mean of the measured flux density values.

TABLE I

The key differential equations stating five variants of the Jiles–Atherton model and numerical complexity assessment.

|   | Model                              | Differential form   | Numerical complexity | Irreversible magnetization $M_{irr}$ (for $c = 0$ )                  |
|---|------------------------------------|---|----------------------|--|
| 1 | Original Jiles–Atherton model [5]  | $\frac{dM}{dH} = \frac{(M_{ah}-M)_\delta}{(1+c)(\delta k - \alpha(M_{ah}-M))} + \frac{c}{1+c}M_\alpha$                            | moderate             | $\frac{dM_{irr}}{dH} = \frac{M_{ah}-M}{\delta k - \alpha(M_{ah}-M)}$ |
| 2 | Modified Jiles–Atherton model [26] | $\frac{dM}{dH} = \frac{(M_{ah}-M)_\delta}{\delta k - \alpha(M_{ah}-M)} + c(1+\alpha)M_\alpha$                                     | moderate             | $\frac{dM_{irr}}{dH} = \frac{M_{ah}-M}{\delta k - \alpha(M_{ah}-M)}$ |
| 3 | Venkataraman model [27]            | $\frac{dM}{dH} = \frac{(M_{ah}-M)_\delta + \delta k c M_\alpha}{\delta k - \alpha(M_{ah}-M)_\delta - \delta k c \alpha M_\alpha}$ | moderate             | $\frac{dM_{irr}}{dH} = \frac{M_{ah}-M}{\delta k - \alpha(M_{ah}-M)}$ |
| 4 | DIMFH model [28]                   | $\frac{dM}{dH} = \frac{(M_{ah}-M)_\delta}{\delta k(1-c)}$   | low                  | $\frac{dM_{irr}}{dH} = \frac{M_{ah}-M}{\delta k}$                    |
| 5 | Xue et al. model [29]              | $\frac{dM}{dH} = \frac{\delta k c M_\alpha + (1-c)(M_{ah}-M)_\delta}{\delta k - \alpha(1-c)(M_{ah}-M)_\delta}$                    | high                 | $\frac{dM_{irr}}{dH} = \frac{M_{ah}-M}{\delta k - \alpha(M_{ah}-M)}$ |

TABLE II

Parameters describing the original Jiles–Atherton model and four modified variants.

|                              | Original Jiles–Atherton model | Corrected Jiles–Atherton model | Venkataraman model    | DIMFH model          | Xue model            |
|------------------------------|-------------------------------|--------------------------------|-----------------------|----------------------|----------------------|
| $M_s$ [A/m]                  | 1 253 676                     | 1 251 250                      | 1 267 751             | 1 218 503            | 1 253 199            |
| $\alpha$                     | $8.8 \times 10^{-5}$          | $9.4 \times 10^{-5}$           | $1.13 \times 10^{-4}$ | $9.2 \times 10^{-5}$ | $8.8 \times 10^{-5}$ |
| $a$ [A/m]                    | 20.05                         | 20.41                          | 23.77                 | $k(1-c) = 3.857$     | 18.41                |
| $k$ [A/m]                    | 16.53                         | 18.42                          | 25.11                 |                      | 17.51                |
| $c$                          | 0.343                         | 0.343                          | 0.343                 | 0.847                | 0.00011              |
| $K_{an}$ [J/m <sup>3</sup> ] | 325.9                         | 338.6                          | 396.9                 | 563.7                | 384.7                |
| $\psi$ [deg]                 | 89.97                         | 89.05                          | 94.44                 | 108.93               | 78.73                |
| $R^2$                        | 0.9910                        | 0.9886                         | 0.9258                | 0.8974               | 0.9913               |

## 5. Results of tests

Five variants of the Jiles–Atherton model were implemented in OCTAVE 10.2 [30]. The parameters of a model were identified during a two-stage parameter identification process. First, the anhysteretic parameters  $M_s$ ,  $a$ ,  $K_{an}$  and the  $\psi$  angle were determined by fitting the anhysteretic magnetization curve. Next, the parameters determining the hysteresis ( $k$  and  $c$ ) were identified during an optimization process based on differential evolution.

Figure 1 presents the experimental hysteresis loop along with simulated curves generated by each of the five variants of the Jiles–Atherton model. The original Jiles–Atherton model and the model updated by Xue reproduce both the steep ascent near saturation and the narrow loop width with high precision, while DIMFH exhibits a marginally wider loop and smoother knee regions.

The optimized parameters for each variant of the Jiles–Atherton model are presented in Table II. All models well describe the shape of a sophisticated hysteresis loop and converged to plausible parameter values. However, differences emerged in both the identified parameter magnitudes and the resulting quality of hysteresis loop reproduction. In particular, the DIMFH model can not distinguish between  $k$  and  $c$  due to the form of the differential equation. In the other model variants,  $c$  is approximately 0.343. Moreover, the Xue model required an extremely low  $c$  value equal  $1.1 \times 10^{-4}$ , indicating that nearly all magnetization changes were treated as irreversible.

The coefficient of determination,  $R^2$ , was used to quantitatively confirm the modelling quality, by comparing the simulated and measured values of the flux density  $B$  in the analyzed quarter of the hysteresis loop  $B(H)$ . The original Jiles–Atherton and Xue models achieved the highest accuracy ( $R^2$  equal

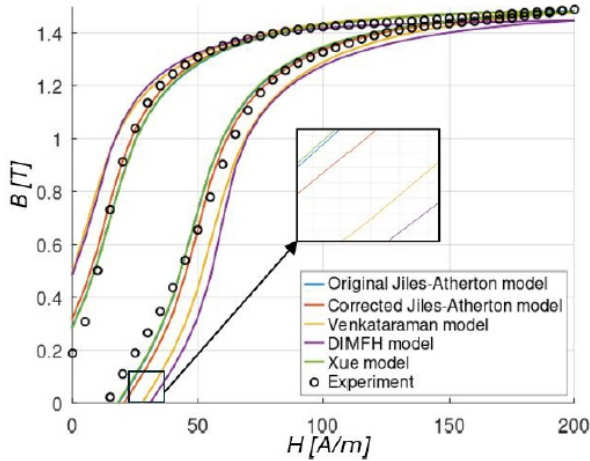


Fig. 1. Comparison of the experimental magnetic hysteresis loop of grain-oriented electrical steel magnetized in the transverse direction with the simulated curves obtained using five variants of the Jiles–Atherton model: original formulation, Cheng correction, Venkataraman modification, DIMFH and Xue update.

to 0.9910 and 0.9913, respectively), closely followed by the Cheng-corrected version ( $R^2 = 0.9886$ ). The Venkataraman and DIMFH models, although still capturing the general loop shape, showed slightly lower agreement ( $R^2 = 0.9258$  and  $R^2 = 0.8974$ , respectively).

## 6. Conclusions

The presented experimental verification of five variants of the Jiles–Atherton model for describing magnetic hysteresis in grain-oriented electrical steel magnetized in the transverse direction indicated that:

- The original Jiles–Atherton model and its Xue variant achieved the highest accuracy with coefficients of determination  $R^2$  of 0.9910 and 0.9913, respectively, successfully reproducing both the steep ascent near saturation and the narrow loop width of grain-oriented electrical steel.
- The Cheng-corrected version demonstrated  $R^2$  of 0.9886, confirming that correcting the convention in the irreversible magnetization equation maintains high predictive capability.
- The Venkataraman and DIMFH modifications showed lower quantitative agreement with  $R^2$  equal to 0.9258 and 0.8974, respectively, but revealed important differences in the description of the magnetization process.
- In DIMFH, the parameters  $k$  and  $c$  cannot be distinguished. In presented research,  $k(1 - c)$  is 3.857.

- The Xue model required an extremely low reversibility coefficient ( $c$  equal to  $1.1 \times 10^{-4}$ ), indicating that in this model, nearly all magnetization changes were considered to be irreversible.

From the perspective of practical applications in electrical power engineering, the choice of modelling variant should consider the numerical complexity relative to the required accuracy. The DIMFH simplification provides the most numerically stable implementation, making it suitable for rapid design iterations. The original Jiles–Atherton model provides an optimal compromise between computational efficiency and accuracy for most engineering applications. The Xue variant, despite its best accuracy, requires a significantly higher level of numerical sophistication.

The presented two-stage parameter identification procedure, which combines separate optimization of anhysteretic and hysteretic parameters through differential evolution, proved to be effective for all tested variants of the Jiles–Atherton model. However, further research should extend the presented comparative analysis to include an investigation focused on dynamic excitation conditions, where frequency-dependent phenomena become the dominant part of the magnetic hysteresis loop behaviour.

To enable reproduction of the presented results and to simplify further research, all scripts used for modelling are available at [www.github.com/romanszewczyk/JAmodel](https://www.github.com/romanszewczyk/JAmodel) in the subdirectory “ModelsComparison”.

## References

- [1] Z.Q. Wu, G. H. Shirkoohi, J.Z. Cao, *J. Magn. Magn. Mater.* **160**, 79 (1996).
- [2] *Nature* **132**, 259 (1933).
- [3] F. Liorzou, B. Phelps, D.L. Atherton, *IEEE Trans. Magn.* **36**, 418 (2000).
- [4] T. Szumiata, P. Rekas, M. Gzik-Szumiata, M. Nowicki, R. Szewczyk, *Materials* **17**, 369 (2024).
- [5] D.C. Jiles, D.L. Atherton, *J. Magn. Magn. Mater.* **61**, 48 (1986).
- [6] A. Jakubas, K. Chwastek, “Modeling Hysteresis Loops of Self-Developed Soft Magnetic Composite Cores Using the Jiles–Atherton–Sablik Theory” (2019).
- [7] X. Wang, D.W.P. Thomas, M. Sumner, J. Paul, S.H.L. Cabral, *IEEE Trans. Magn.* **44**, 340 (2008).
- [8] S. Cundeva, *Serb. J. Electr. Eng.* **5**, 21 (2008).
- [9] K. Górecki, K. Detka, *Mater. Sci. Eng. B* **177**, 1248 (2012).

- [10] P.D. Dimitropoulos, G.I. Stamoulis, E. Hristoforou in: *Proc. of IEEE Sensors*, IEEE, 2004, p. 1566.
- [11] Y. Liu, X. Gao, Y. Li, . *Sens. Actuators A Phys.* **250**, 7 (2016).
- [12] Y. Li, J. Zhu, L. Zhu, Y. Li, G. Lei, *IEEE Trans. Magn.* **56**, 7511405 (2020).
- [13] M. Sierżęga, W. Mazgaj, *Arch. Electr. Eng.* **72**, 855 (2023).
- [14] N.C. Pop, O.F. Caltun, *Acta Phys. Pol. A* **120**, 491 (2011).
- [15] R. Szewczyk, *Materials* **7**, 5109 (2014).
- [16] Z. Jakšić, S. Devi, O. Jakšić, K. Guha, *Biomimetics* **8**, 278 (2023).
- [17] R. Szewczyk, in: *Automation 2018*, Vol. 743, Eds. R. Szewczyk, C. Zieliński, M. Kaliczyńska, Springer, Cham 2018.
- [18] F. Qiu, W. Ren, G.Y. Tian, Y. Gao, B. Gao, in: *2015 IEEE Far East NDT New Technology & Application Forum (FENDT)*, IEEE 2015, p. 207.
- [19] O. Perevertov, R. Schäfer, *Mater. Res. Express* **3**, 096103 (2016).
- [20] A. Ramesh, D.C. Jiles, Y. Bi, *J. Appl. Phys.* **81**, 5585 (1997).
- [21] A.P. Baghel, S.V. Kulkarni, *J. Appl. Phys.* **113**, 043908 (2013).
- [22] F.T. Calkins, R.C. Smith, A.B. Flatau, *IEEE Trans. Magn.* **36**, 429 (2000).
- [23] J.H.B. Deane, *IEEE Trans. Magn.* **30**, 2795 (1994).
- [24] J.R. Dormand, P.J. Prince, *Celest. Mech.* **18**, 223 (1978).
- [25] R. Storn, K. Price, *J. Glob. Optim.* **11**, 341 (1997).
- [26] R. Szewczyk, P. Cheng, *Acta Phys. Pol. A* **133**, 654 (2018).
- [27] R. Venkataraman, P.S. Krishnaprasad, in: *Proc. of the 37th IEEE Conf. on Decision and Control (Cat. No.98CH36171)*, IEEE, 1998, p. 2443.
- [28] J. Pytlík, J. Luňáček, O. Životský, *Phys. Review B* **108**, 104414 (2023).
- [29] G. Xue, P. Zhang, Z. He, D. Li, Z. Yang, Z. Zhao, *Commun. Comput. Phys.* **21**, 763 (2017).
- [30] J.W. Eaton, *J. Process Control* **22**, 1433 (2012).